

Scientific paper

# Estimating Mean Crystallite Size of Magnetite using Multivariate Calibration and Powder X-ray Diffraction Analysis

Maykon A. Lemes,<sup>1</sup> Mariana S. Godinho,<sup>1</sup> Denilson Rabelo,<sup>1</sup> Felipe T. Martins,<sup>1</sup> Alexandre Mesquita,<sup>2</sup> Francisco N. De Souza Neto,<sup>3</sup> Olacir A. Araujo,<sup>3</sup> and Anselmo E. De Oliveira<sup>1,\*</sup>

<sup>1</sup> Instituto de Química, UFG, PO Box 131, Goiânia, GO, 74001-970, Brazil

<sup>2</sup> UNIFAL, Rua Gabriel Monteiro da Silva, 700, Alfenas, MG, 37130-000, Brazil

<sup>3</sup> UnUCET, UEG, PO box 459, Anápolis, GO, 75000-000, Brazil

\* Corresponding author: E-mail: [elcana@ufg.br](mailto:elcana@ufg.br)

Received: 25-03-2014

## Abstract

Powder X-ray diffraction patterns for 29 samples of magnetite, acquired using a conventional diffractometer, were used to build PLS calibration-based methods and variable selection to estimate mean crystallite size of magnetite directly from powder X-ray diffraction patterns. The best IPLS model corresponds to the Bragg reflections at 35.4° (h k l = 3 1 1), 43.0° (h k l = 4 0 0), 53.6° (h k l = 4 2 2), and 57.0° (h k l = 5 1 1) in 2 $\theta$ . The best model was a GA-PLS which produced a model with RMSEP of 0.9 nm, and a correlation coefficient of 0.9976 between mean crystallite sizes calculated using Williamson-Hall approach and the ones predicted by GA-PLS method. These results indicate that magnetite mean crystallite sizes can be predicted directly from Powder X-Ray Diffraction and multivariate calibration using PLS variable selection approach.

**Keywords:** Crystallite size, GA-PLS, Powder X-ray; magnetite.

## 1. Introduction

Powder X-ray and neutron diffraction analyses are useful for many purposes, such as structure determination, phase identification and quantification in solid mixtures, estimate of preferred orientation effects, lattice microstrain and mean crystallite size.<sup>1–6</sup> Furthermore, powder diffraction techniques do not need prior hard steps of sample preparation. For instance, sometimes only grinding procedures are enough to avoid preferred orientation of crystallites. Such techniques also are commonly non-destructive when dealing with ceramics and inorganic materials.

Even though powder diffraction can provide helpful knowledge on solid state properties, one can realize that specialized data handling from X-ray (or neutron) diffraction experiment is needed in order to find meaningful correlations with target features. Nowadays, software packages, as, for instance, GSAS,<sup>7</sup> TOPAS,<sup>8</sup> and PM2K<sup>9</sup> allow

for simultaneous structural, quantitative, and morphological analyses using the Rietveld method. In these programs, both background and peak profiles are fitted using high-order polynomial and pseudo-Voigt shape functions with refinement of low-angle asymmetry parameters even for estimating crystallite size. Crystallite size and lattice strain can be also analyzed with software developed exclusively for these purposes, such as BREADTH,<sup>7</sup> using simplified and double-Voigt integral-breadth methods, and XBROAD,<sup>8</sup> based on classical methods as Williamson–Hall and Warren–Averbach ones.

Based on powder X-ray diffraction (PXRD) data, crystallite size of iron oxide particles is commonly estimated using the Scherrer equation from a single diffraction peak as the most intense ones.<sup>13</sup> However, no analytical standardization about what peaks should be taken for calculation and how to deal with them is found in literature, besides Scherrer approximation does not account for

microstrain-related broadening and, therefore, only provides rough estimates. Besides, some researches have dealt with multivariate analysis and PXRD,<sup>14–18</sup> but publications concerning magnetite mean crystallite size estimates by PXRD and Partial Least Squares (PLS) calibration have not been reported yet.

In this way, we were concerned in developing an alternative approach to determine the mean crystallite size of iron oxide nanoparticles based on PXRD which could provide standardization parameters for diffraction pattern analysis besides to take advantage of direct crystallite size estimate even from samples featured by the presence of extra crystalline and non-crystalline phases and wide size distribution. For this purpose, this manuscript describes a PLS calibration-based method using variable selection to estimate mean crystallite size of magnetite directly from powder X-ray diffraction patterns of iron oxide samples prepared under a wide variety of synthetic conditions

## 2. Materials and Methods

### 2.1. Sample Preparations

In order to obtain magnetite in different sizes and varied chemical environments we prepared 29 samples which can be divided in two principal groups: I) magnetite nanoparticles (N) prepared by coprecipitation of Fe<sup>2+</sup> and Fe<sup>3+</sup> ions from alkaline aqueous solutions;<sup>19</sup> II) nanocomposites of magnetite and sulfonated styrene-divinylbenzene (Sty-DVB) copolymers (NC).<sup>20–22</sup> The alkaline coprecipitation of Fe<sup>2+</sup> and Fe<sup>3+</sup> is the most common method for producing magnetite nanoparticles. In a typical recipe, 500 mL of solution containing 0.05 molL<sup>-1</sup> of Fe<sup>2+</sup> and 0.10 molL<sup>-1</sup> Fe<sup>3+</sup> were added to 170 mL of alkaline solution containing 1.5

molL<sup>-1</sup> of hydroxide under mechanical stirring and heating. In this work, the stirring speed, the temperature and the hydroxide type (KOH, NaOH, and NH<sub>4</sub>OH) are some of the factors which were changed in order to produce nanoparticles with different sizes. All nanoparticles were prepared with the respective iron sulphate salts.

The nanocomposite samples are microspheres (100–250 μm) of sulfonated Sty-DVB copolymer with magnetite nanoparticles dispersed in the polymeric matrix or in the porous structure. The nanocomposite preparation followed a three-step procedure (one full chemical cycle). First, the sulfonated polymeric spheres were mixed with the bath solution containing Fe<sup>2+</sup> and stirred for 1 h, at room temperature. Second, the polymer particles were separated by filtration and washed thoroughly with water

**Table 1.** Experimental synthesis conditions of magnetite nanoparticles (N).

Sample	Speed Stirring /rpm	Coprecipitation Temperature/ °C	Hydroxide type	Size/nm
N1	200	30	KOH	6.1
N2	400	30	KOH	2.7
N3	200	50	KOH	9.2
N4	400	50	KOH	8.7
N5	200	30	NaOH	13.0
N6	400	30	NaOH	9.0
N7	200	50	NaOH	8.1
N8	400	50	NaOH	9.4
N9	300	40	NH <sub>4</sub> OH	6.4
N10	300	40	NH <sub>4</sub> OH	12.9
N11	300	20	NH <sub>4</sub> OH	8.5
N12	300	40	NH <sub>4</sub> OH	7.2
N13	300	35	KOH	9.0

**Table 2.** Experimental synthesis conditions of magnetite/Sty-DVB copolymer nanocomposites (NC).

Sample	Porous Structure Type	Surface Area/m <sup>2</sup> g <sup>-1</sup>	[Fe <sup>2+</sup> ]/mmolL <sup>-1</sup>	Cycles	Size /nm
NC1	Gel	0	80	3	14.5
NC2	Gel	0	300	3	16.3
NC3	Meso/collapsed	0.6	220	3	28.1
NC4	Meso/collapsed	0.6	300	3	25.2
NC5	Macro/collapsed	1.5	220	3	25.4
NC6	Macro/collapsed	1.5	300	3	28.9
NC7	Macroporous	69	220	1	31.7
NC8	Macroporous	69	220	2	28.4
NC9	Macroporous	69	220	3	28.0
NC10	Macroporous	69	220	4	27.7
NC11	Macroporous	69	300	4	32.9
NC12	Macroporous	69	220	4 <sup>a</sup>	27.4
NC13	Macroporous	69	220	4 <sup>b</sup>	30.4
NC14	Macroporous	269	220	3	24.9
NC15	Macroporous	269	220	4	24.9
NC16	Macroporous	269	220	4 <sup>a</sup>	30.2

<sup>a</sup>. Cycles performed without washing Fe<sup>2+</sup> ions not linked to sulfonic groups (step II).

<sup>b</sup>. Nanocomposite with oleic acid adsorbed on magnetite nanoparticles.

until no iron was detected in the eluent. Third, the alkaline oxidation of the  $\text{Fe}^{2+}$  ions linked to sulfonic groups was performed by treating the ferrous-loaded resin with aqueous solution containing potassium hydroxide and sodium nitrate at 70 °C for 15 min, under stirring.

The nanoparticle size and magnetite concentration in the composite was conveniently controlled by changing the number of chemical cycles, the porosity type of Sty-DVB copolymer (gel, mesoporous, and macroporous), and the  $\text{Fe}^{2+}$  ions concentration in charge solution copolymers.<sup>20–22</sup> Some composites were prepared without washing free  $\text{Fe}^{2+}$  ions inside copolymer porous structure, i.e., without step II. Tables 1 and 2 show synthesis conditions of the magnetite nanoparticles (N) and magnetite/sulfonated Sty-DVB copolymer nanocomposites (NC), respectively.

## 2. 2. PXRD Analysis

Twenty nine samples obtained after drying of magnetite nanoparticles and nanocomposites were mounted on a sample holder (grooved glass slide) and exposed to X-ray beam (graphite monochromatized  $\text{CuK}\alpha$  radiation,  $\lambda = 0.15418$  nm) generated at 40 kV and 30 mA on a Shimadzu XRD-6000 diffractometer. All PXRD patterns were acquired at room temperature under continuous scan mode (scan axis  $\theta$ - $2\theta$  with scan speed 1.000°/min). Intensity data were measured at each 0.020° in a  $2\theta$  range between 10° and 80°. Divergence and scattering slits were set at 1.000°, as well as receiving slit (0.300 mm) and counter monochromator were employed for data acquisition. No standard powder was used to determine instrumental resolution function. The program Search Match, from Shimadzu XRD-6000 v4.1 was employed to monitor the data acquisition.

Prior to input the experimental powder X-ray diffraction patterns of the samples in the multivariate calibration procedure, they were indexed with the data base PDF-2 data base (International Center for Diffraction Data-ICDD), entry number 880866, which has allowed us to identify the magnetite phase of  $\text{Fe}_3\text{O}_4$  from powder X-ray diffraction data. Other crystal phases could be also identified in some X-ray diffraction patterns (see Results and Discussion section).

The  $2\theta$  values were not expressed as d-values because all diffraction patterns were acquired using  $\text{CuK}\alpha$  radiation. Therefore, the X-ray patterns were dealt as acquired, except for normalization of all intensities against the most intense one of each diffraction pattern. For each sample, a file containing normalized intensity data as a function of raw  $2\theta$  positions step rose by 0.020° in  $2\theta$  were generated.

## 2. 3. Williamson-Hall Method

The average crystallite size of the samples was determined from the FWHM of the diffraction peaks accor-

ding to Williamson-Hall equation.<sup>23</sup> The FWHM of any diffraction peak can be described as a linear combination of the contributions from the lattice strain and the crystallite size through the Williamson-Hall relation

$$\frac{\beta}{\lambda} \cos\theta = \frac{k}{D} + \frac{4\varepsilon}{\lambda} \sin\theta \quad (1)$$

where  $\beta$  is the diffracted FWHM (in radians),  $\lambda$  the incident wavelength,  $\theta$  the Bragg angle,  $D$  the average crystallite and  $\varepsilon$  the microstrain. A  $K$  value of 0.9 was used. This value is considered as a good average value for small uniformly spherical crystals as those of magnetite domains.<sup>24,25</sup> The slope and the intercept of the axis in the plot of  $(\beta\cos\theta)/\lambda$  versus  $\sin\theta$  provide the microstrain value and the mean crystallite size, respectively. Lorentzian function was used to determine the FWHM of diffraction peaks. For all samples, X-ray diffraction peak positions and FWHM of the Bragg reflections (2 2 0), (3 1 1), (4 0 0), (5 1 1) and (4 4 0) at approximately 30.1°, 35.4°, 43.0°, 57.1° and 62.3° in  $2\theta$ , respectively, were used into the Williamson-Hall analysis.

## 2. 4. Data Treatment

PXR diffraction patterns were converted to ASCII format files using the program Search Match, from Shimadzu XRD-6000 v4.1, and then loaded into the Matlab software.<sup>26</sup> All diffraction patterns were represented by a  $29 \times 3501$  data matrix whose 29 individual lines correspond to the diffraction patterns of different samples and whose 3501 columns contain normalized intensities for each  $2\theta$  scattering angle. Samples were divided according to Kennard-Stone sampling algorithm<sup>27</sup> in 20 and 9 for the calibration and validation sets, respectively. Mean crystallite sizes estimated from Williamson-Hall method were used in both calibration and validation sets.

Multivariate data analyses were treated in Matlab using PLS Toolbox software<sup>28</sup> and in-house algorithms. For PLS and Interval PLS (IPLS), forward and backward, the intensities were mean-centered, preprocessed using Savitzky-Golay smoothing filter and first derivative with a window width of 15 points and second degree polynomial in order to reduce the noise. Genetic Algorithm (GA) combined with PLS (GA-PLS) regression used a starting population of 200 chromosomes and 350 variables, 10% mutation probability, 90% cross-over probability, and 200 generations.

### 2. 4. 1. PLS Model and PXRD Data

PLS regression algorithm was applied to the PXRD data of the magnetite nanoparticles and nanocomposites to estimate mean crystallite sizes. The  $\mathbf{X}$  data matrix containing the PXRD information (line = intensity signal; column =  $2\theta$  position), and the nanoparticle mean size data

distribution,  $\mathbf{Y}$ , were modelled by linear latent variables according to the regression models

$$\mathbf{X} = \mathbf{T}\mathbf{P}^T + \mathbf{E}_X \quad (2)$$

$$\mathbf{Y} = \mathbf{U}\mathbf{Q}^T + \mathbf{E}_Y \quad (3)$$

where the matrices  $\mathbf{T}$  and  $\mathbf{U}$  are the score matrices,  $\mathbf{P}$  and  $\mathbf{Q}$  are the loading matrices, and  $\mathbf{E}_X$  and  $\mathbf{E}_Y$  are the residual matrices. The columns of  $\mathbf{T}$  and  $\mathbf{U}$  provide a new representation of  $\mathbf{X}$  and  $\mathbf{Y}$  in an orthogonal space. The  $x$ - and  $y$ -scores are connected by the inner linear relationship

$$\mathbf{U} = \mathbf{T}\mathbf{D} + \mathbf{H} \quad (4)$$

with  $\mathbf{H}$  and  $\mathbf{D}$  being the residual and regression matrices, respectively. References 29 and 30 provide more details of the PLS method. As a result, predicted values of the observed variables can be computed from the  $\mathbf{X}$  data matrix containing X-ray data.

PLS is a valuable tool for calibration using a small range or the entire diffraction pattern. However, when combined with variable selection it can result in diffraction pattern subsets with smaller prediction errors and a better correlation between the expected and real parame-

ter. Among the variable selection methods, GA is an advanced tool for factor-based regression methods like PLS (GA-PLS),<sup>31</sup> and the mathematical method IPLS is a PLS interactive extension.<sup>32,33</sup>

In the GA-PLS model the variables are selected according to a stochastic search technique based on classical operators like select-copy, cross-over and mutation build to mimic the evolution of species according to Darwin's theory of evolution.<sup>34</sup> For the IPLS model the X-ray data set is divided in a certain number of intervals, and PLS models are built for each of these intervals. The root mean squared error of calibration (RMSEC) and the root mean squared error of prediction (RMSEP) are common statistical parameters used as criteria for judging the performance of multivariate calibration model.<sup>35,36</sup>

### 3. Results and Discussion

The multivariate calibration PLS method was tested for prediction of magnetite mean crystallite size directly from PXRD data. For this purpose, twenty nine samples of magnetite synthesized under different conditions as described in Materials and Methods section were analyzed by PXRD technique. Figure 1 shows diffraction patterns of

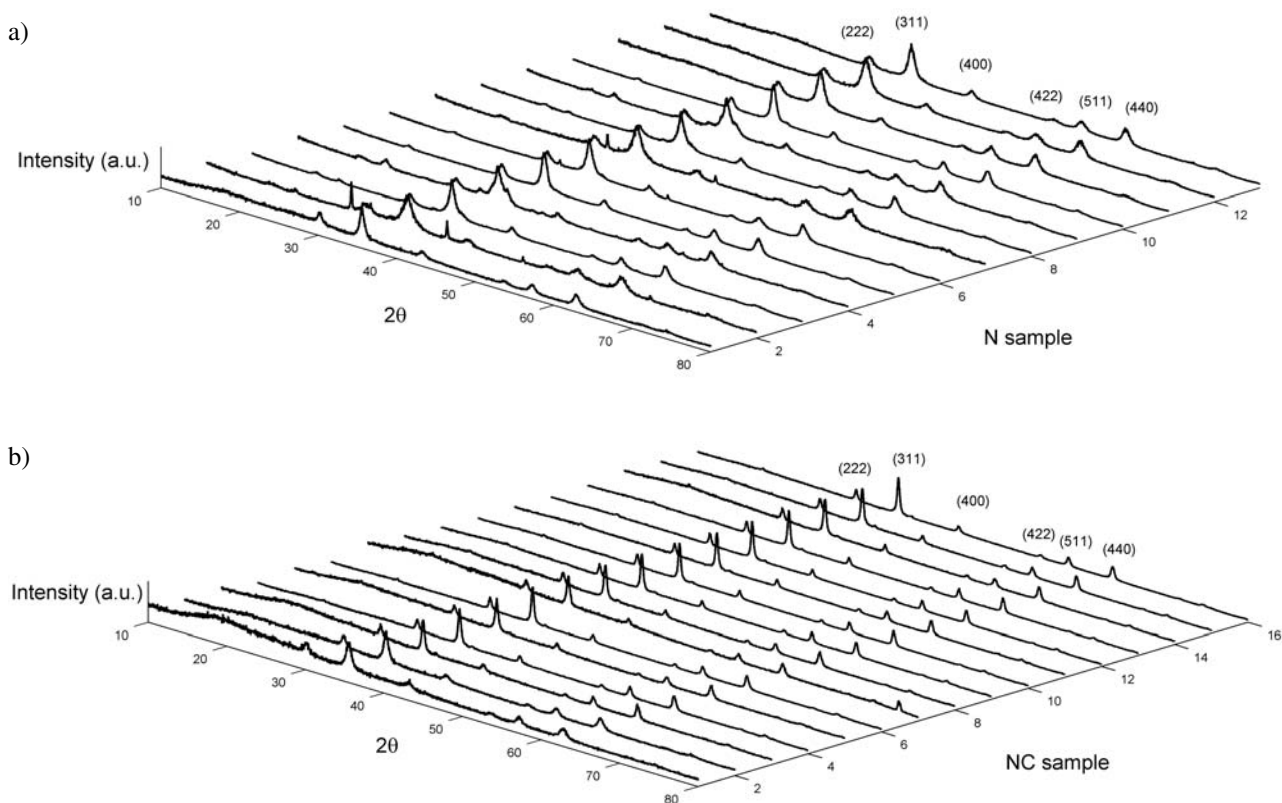


**Fig. 1.** Powder X-ray diffraction patterns of twenty nine magnetite samples (continuous lines) synthesized as described in Materials and Methods section, and of a reference diffraction pattern (numbers in parenthesis) of the same crystal phase (PDF number 880866): (a) nanoparticle (N) samples ordered according to Table 1, and (b) nanocomposite (NC) samples ordered according to Table 2; Intensities in arbitrary units (a.u.).

magnetite nanoparticles (N) synthesized by coprecipitation of  $\text{Fe}^{3+}$  and  $\text{Fe}^{2+}$  ions from alkaline solutions (Figure 1a) and magnetite/sulfonated Sty-DVB copolymer nanocomposites (NC) (Figure 1b). All X-ray diffractograms have characteristic profiles of magnetite with peaks at angles  $18.3^\circ$ ,  $30.1^\circ$ ,  $35.4^\circ$ ,  $37.0^\circ$ ,  $43.0^\circ$ ,  $53.6^\circ$ ,  $57.1^\circ$  and  $62.3^\circ$  corresponding to planes (1 1 1), (220), (311), (222), (400), (422), (511) and (440), respectively (PDF 880866).

The magnetite nanoparticles presented contaminants and another iron oxide phase differently of nanocomposite samples. Sample N2 showed peaks at  $28.5^\circ$ ,  $41.8^\circ$ , and  $50.8^\circ$  corresponding to planes (022), (042), and (321) of potassium sulphate (PDF 850939). The presence of this salt can be justified by the use of iron sulphates and potassium hydroxide in the nanoparticles synthesis. Samples N2, N4 and N9 presented a peak at  $21.2^\circ$  corresponding to plane (110) of goethite (PDF 810462). Goethite is an intermediate in hydrothermal synthesis of magnetite from  $\text{Fe}^{3+}$  and  $\text{Fe}^{2+}$  alkaline solutions which can be not completely converted at low temperatures. Samples N6 and N7 showed peaks at  $32.8^\circ$  and  $47.1^\circ$  corresponding to planes (200) and (220) of sodium chloride (PDF 831728) which presence can be justified by the use of hydrochloric acid to stabilize  $\text{Fe}^{2+}$  solutions and sodium hydroxide in the magnetite synthesis.

The differences in the nanoparticle sizes between N and NC samples can be attributed not only to the effect of the polymeric template but also to the use of different types of iron ions. In a previous paper, we have showed that manganese ferrite nanoparticles prepared from  $\text{Fe}^{3+}$  and  $\text{Mn}^{2+}$  ions have smaller sizes than nanoparticles prepared from  $\text{Fe}^{2+}$  and  $\text{Mn}^{2+}$  ions.<sup>38</sup> The different conditions for the preparation of magnetite/sulfonated Sty-DVB copolymer nanocomposites allow the control of the size and amount of nanoparticles. One way to make this control is changing the porosity of Sty-DVB copolymer which varied from a gel type, i.e., non porous in dry state to a macroporous type with high surface area.<sup>20,21</sup> Some intermediate porous structures presented collapsed pores due drying and/or sulfonation processes.<sup>39,40</sup> Since the sulfonated copolymers are hydrophilic, the collapsed pores can re-expand at the moment of  $\text{Fe}^{2+}$  conversion to magnetite inside microspheres. In general, the size and the amount of nanoparticles in the nanocomposites increase with the increasing of  $\text{Fe}^{2+}$  ion concentration and the number of

charge/oxidation cycles.<sup>21</sup> Samples NC1, NC3, NC5, and NC7 presented an amorphous halo centred at approximately  $20^\circ$  in  $2\theta$  characteristic of amorphous polystyrene.<sup>41</sup> The amorphous halo tended to disappear with the increasing of magnetite concentration in the nanocomposite.

Samples were divided according to Kennard-Stone sampling in 20 and 9 for the calibration and validation sets, respectively. The nanoparticle sizes ranged from 2.7 to 32.9 nm. For calibration and validation sets it ranged from 2.7 to 32.9 nm, and 6.4 to 30.4 nm, respectively. The PLS model was obtained using all 3501 variables, ranging from  $10^\circ$  to  $80^\circ$ . According to the lowest RMSEC of 1.8 nm, having four latent variables, this model showed a RMSEP of 2.9 nm for the magnetite mean crystallite size, and a squared product-moment correlation coefficient of prediction,  $r_{pred}^2$ , of 0.9385, Table 3.

Diffraction pattern interval selection was first carried out by IPLS. Regions were used to split the diffraction patterns, and to construct a PLS regression model for each interval. These models, IPLS1 and IPLS2, resulted in RMSEP of 2.7 and 3.1 nm, Table 3, presenting a squared product-moment correlation coefficient of 0.9577 and 0.9750, respectively. The IPLS models intervals correspond to the most intense Bragg reflection at  $35.4^\circ$  in  $2\theta$  (h k l = 3 1 1), and to the reflections at  $43.0^\circ$  (h k l = 4 0 0),  $53.6^\circ$  (h k l = 4 2 2), and  $57.1^\circ$  (h k l = 5 1 1). In agreement with the practice of selecting the (3 1 1) peak for inputting its X-ray diffraction peak position and FWHM parameters into the Scherrer equation, our IPLS results demonstrate that this peak indeed correlates better with particle size estimate than others. In fact, the (3 1 1) peak is commonly used in the Scherrer equation for calculation of particle size of magnetite. As a general rule applying to selection of a single Bragg peak to be used in the Scherrer equation, the most intense diffraction reflections lying in the  $2\theta$  range between  $30^\circ$  and  $50^\circ$  are chosen, often getting better estimate results of particle size than low-angle asymmetric peaks below  $30^\circ$  in  $2\theta$ . Furthermore, both partial models have reflected the fact that crystallite size effect on peak width is better observed at middle and high-angle reflections, which are less affected by low-angle asymmetry effects, since lower crystallite size prediction errors and higher correlations between predicted and estimated (from Williamson-Hall method) mean sizes were obtained by using peaks above  $30^\circ$ . More precisely, Bragg peaks at

**Table 3.** Statistical results for all PLS based multivariate calibration models.

Model	$2\theta$ range	NV <sup>a</sup>	LV <sup>b</sup>	RMSEC/nm	RMSEP/nm	$r_{pred}^2$
PLS	$10^\circ$ – $80^\circ$	3501	4	1.8	2.9	0.9385
IPLS1	$34.02^\circ$ – $58.00^\circ$	1200	4	2.2	2.7	0.9577
IPLS2	$31.02^\circ$ – $38.00^\circ$ $52.02^\circ$ – $59.00^\circ$	700	5	1.4	3.1	0.9750
GA-PLS	$10^\circ$ – $80^\circ$	132	7	0.1	0.9	0.9972

<sup>a</sup> Total number of variables. <sup>b</sup> Optimum number of latent variables.

higher angles reflect better the crystallite size than those at lower angles using the IPLS models aforementioned. This can be a consequence of the anisotropy of size-strain line broadening, *i.e.*, it depends on the  $hkl$  reflection. In cation-substituted ferrites, X-ray line broadening due to the size and strain effects has been reported to be isotropic and anisotropic, respectively, such as in zinc,<sup>42,43</sup> manganese,<sup>42,43</sup> and lithium ferrite phases, as well as in Zn, Ni ferrite/NiO nanocomposites<sup>45</sup> and in nanocrystalline magnetite with rare earth ions substitution, namely, Gd, Dy, Ho, Tm, and Yb.<sup>46</sup> However, anisotropy in both size and strain X-ray line broadening does occur for magnesium,<sup>47</sup> yttrium,<sup>48</sup> and indium<sup>48</sup> ferrite nanoparticles. Even though size anisotropy for non-substituted magnetite is small ( $114 \pm 9 \text{ \AA}$ ),<sup>48</sup> it can not be neglected and its effect in the multivariate calibration could be observed in the better statistical scores for middle and high-angle X-ray peaks. Similarly, instrumental broadening is a function of the diffraction angle,<sup>49</sup> which can also help us to rationalize the higher model merits for the Bragg peaks above  $30^\circ$ . Therefore, the method developed in this study takes advantage in decreasing the instrumental and strain effects in broadening of middle and high-angle peaks which mostly bring themselves the size contribution.

GA-PLS model was also obtained for the magnetite samples using 132 variables, Figure 2, and it provided the more accurate particle size prediction and the better correlation, as it can be seen in Table 3 and in Figure 3. The best model presented RMSEP of 0.9 nm and  $r^2_{pred}$  of 0.9972. This model has accounted both the low-angle peak at  $18.3^\circ$  ( $hkl = 111$ ) as the middle and high-angle ones scored with iPLS models plus the (622) reflection at  $75.0^\circ$ . All Bragg peaks used to estimate the input mean sizes with the Williamson-Hall analysis were taken by GA-PLS model. This suggests that the estimate of magnetite crystallite size is most precise when exploring the peak broadening information coded in several reflections instead of the single-peak approach using the Scherrer formula.

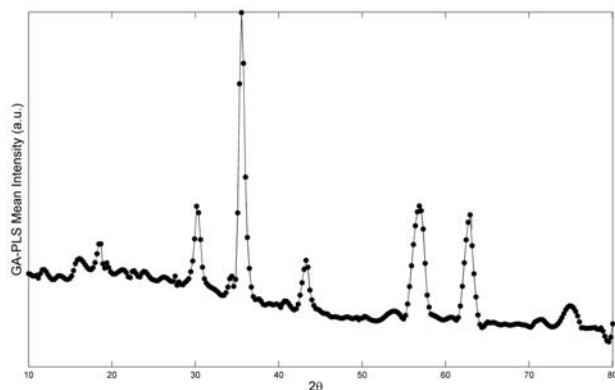


Fig. 2. GA-PLS mean intensities versus  $2\theta$  angles for the 132 variables (●) applied to the magnetite PXRD diffraction patterns. Intensities in arbitrary units (a.u.).

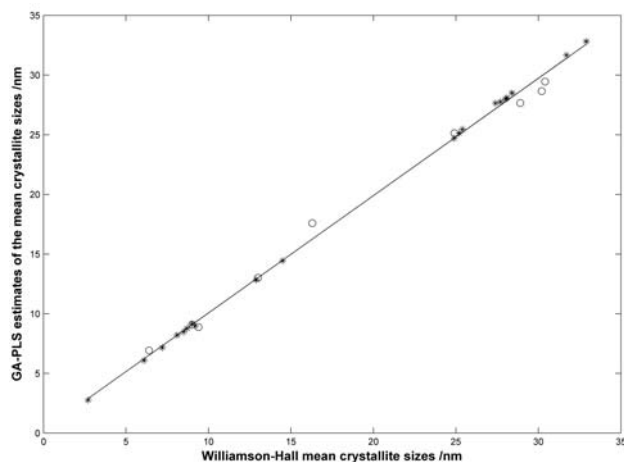


Fig. 3. Comparison of magnetite mean crystallite sizes calculated from Williamson-Hall analysis and its GA-PLS estimates. The solid line represents a linear fit. (\*) calibration samples; (O) validation samples.

In Figure 3 the correlation between mean crystallite sizes calculated by Williamson-Hall estimate and the ones estimated by the best GA-PLS calibration model is shown. The linear fit presents an excellent  $r^2$  of 0.9976. In the overall, RMSEP values obtained here are lower than 15% that can be expected when using such approach for samples having mean size of less than 100 nm.<sup>50</sup> The low RMSEP value of 0.9 nm for the best PLS model (GA-PLS) indicates that magnetite mean crystallite sizes can be predicted directly from PXRD and multivariate calibration using PLS variable selection approach. As a result, GA-PLS is able to detect relevant regions in the X-ray data set that correlate with mean crystallite sizes.

## 4. Conclusions

The multivariate calibration method was successfully employed for the estimate of mean size of magnetite crystallite directly from powder X-ray diffraction patterns. Our variable selection approaches revealed that the most intense (311) peak is the best model when a single interval is used, in agreement with the common practice of selecting this Bragg reflection for magnetite particle size calculation by the Scherrer equation. However, a still better model using GA-PLS was obtained, providing a more precise particle size prediction that correlates with the most powder X-ray diffraction data of magnetite in a similar way of the Williamson-Hall method using several peaks to estimate particle size averages. Therefore, our multivariate calibration approach was able to relate the crystallite size to X-ray diffraction peaks away from the low angle region affected mainly by instrument-related asymmetry.

A small amount of magnetite sample is needed for data acquisition on a conventional powder X-ray diffrac-

tometer, besides the method developed in this study is also robust, direct, rapid, non-destructive, and it allows for a timely and practical crystallite size estimate alternatively to software tools using Rietveld codes even in the presence of extra phases (crystalline or not) and wide size distribution.

As a consequence of this study, we believe that the multivariate calibration method can be better explored for estimate of crystallite size and other solid state properties of different crystal phases using X-ray data.

*Acknowledgement(s). Financial support from the CNPq is gratefully acknowledged. M.S.G. thanks CNPq for Doctoral fellowship, and M.A.L. thanks CAPES for Master fellowship.*

## 5. References

- Z. Nemet, G. C. Kis, G. Pokol, A. Demeter, *J. Pharm. Biomed. Anal.* **2009**, *49*, 338–346.
- A. Kulczycki, *Chem. Anal.* **2000**, *45*, 305–310.
- V. Pecharsky, P. Zavalij, The Powder Diffraction Pattern, in: V. Pecharsky, P. Zavalij (Eds.), *Fundamentals of Powder Diffraction and Structural Characterization of Materials*, 2nd ed., Springer, New York, **2009**, pp 151–201.
- C. Giacobozzo, H. L. Monaco, G. Artioli, D. Viterbo, M. Milanesio, G. Gilli, P. Gilli, G. Zanotti, G. Ferraris, M. Catti (Eds.), *Fundamentals of Crystallography*, 3rd ed., Oxford University Press, Oxford, **2011**.
- R. Jenkins, R. L. Snyder, *Introduction to X-Ray Powder Diffraction*, Wiley-Interscience, New York, **1996**.
- R. A. Young, *The Rietveld method*, Oxford University Press, New York, **1993**.
- A. C. Larson, R. B. von Dreele, Los Alamos National Laboratory Report LAUR, **2000**.
- Bruker. TOPAS. Version 4. Karlsruhe, Bruker AXS, **2000**.
- M. Leoni, T. Confente, P. Scardi. *Kristallogr.* **2006**, *23*, 249–254.
- H. M. Rietveld, *J. Appl. Crystallogr.* **1969**, *2*, 65–71.
- D. Balzar, *J. Appl. Cryst.* **1995**, *28*, 244–245.
- Z. Skoko, J. Popovic, K. Dekanic, V. Kolbas, S. Popovic, *J. Appl. Cryst.* **2012**, *45*, 594–597.
- Y. Masabuchi, Y. Sato, A. Sawada, T. Motohashi, H. Kiyono, S. Kikkawa, *J. Eur. Ceram. Soc.* **2011**, *31*, 2459–2462.
- M. Harju, P. Minkkinen, J. Valkonen, *Chemom. Intell. Lab. Syst.* **1994**, *23*, 341–350.
- L. J. Janik, J. O. Skjemstand, M. D. Raven, *Australian Journal of Soil Research* **1995**, *33*, 621–636.
- D. Lee, H. Lee, C. H. Jun, C. H. Chang, *Appl. Spectrosc.* **2007**, *61*, 1398–1403.
- M. Suda, K. Takayama, M. Otsuka, *Anal. Sci.* **2008**, *24*, 451–457.
- M. Norrman, K. Stahl, G. Schulckebier, S. Al-Karadaghi, *J. Appl. Crystallogr.* **2006**, *39*, 391–400.
- R. Valenzuela, M. C. Fuentes, C. Parra, J. Baeza, N. Duran, S. K. Sharma, M. Knobel, J. Freer, *J. Alloys Comp.* **2009**, *488*, 227–231.
- D. Rabelo, S. S. Andrade, V. K. Garg, A. C. Oliveira, P. C. Morais, *J. Magn. Magnet. Mater.* **2005**, *289*, 25–27.
- D. Rabelo, P. C. Morais, R. B. Azevedo, E. C. D. Lima, *Chem. Mater.* **2003**, *15*, 2485–2487.
- D. Rabelo, E. C. D. Lima, A. C. Reis, W. C. Nunes, M. A. Novak, V. K. Garg, P. C. Morais, *Nano Letters* **2001**, *1*, 105–108.
- G. K. Williamson, W. H. Hall, *Acta Metall.* **1953**, *1*, 22–31.
- H. P. Klug, L.E. Alexander, *Procedures for Polycrystalline and Amorphous Materials*, 2nd ed., John Wiley and Sons, New York, **1974**.
- J. G. Deng, C. L. He, Y. X. Peng, J. H. Wang, X. P. Long, P. Li, A. S. C. Chan, *Synthetic Met.* **2003**, *139*, 295–301.
- Matlab v7.14.0.739, The MathWorks Natick, USA.
- R. W. Kennard, L. A. Stone, *Technometrics* **1969**, *111*, 137–148.
- PLS Toolbox v6.2, Eigenvector Research Inc., USA.
- S. Wold, M. Sjostrom, L. Eriksson, *Chemom. Intell. Lab. Syst.* **2001**, *58*, 109–130.
- K. Varmuza, P. Filzmoser, *Introduction to Multivariate Statistical Analysis in Chemometrics*, CRC Press, Boca Raton, **2009**.
- D. Broadhurst, R. Goodacre, A. Jones, J. J. Rowland, D. B. Kell, *Anal. Chim. Acta* **1997**, *348*, 71–86.
- A. Borin, R. J. Poppi, *Vib. Spectrosc.* **2005**, *37*, 27–32.
- L. Norgaard, A. Saudland, J. Wagner, J. P. Nielsen, L. Munck, S. B. Engelsen, *Appl. Spectrosc.* **2000**, *54*, 413–419.
- A. L.-S. Chua, N. A. Benedek, L. Chen, M. W. Finnis, A. P. Sutton, *Nat. Mater.* **2010**, *9*, 418–422.
- R. Leardi, L. Norgaard, *J. Chemom.* **2004**, *18*, 486–497.
- S. D. Osborne, R. B. Jordan, R. Künnemeyer, *Analyst* **1997**, *122*, 1531–1537.
- N. Mizutani, T. Iwasaki, S. Watano, T. Yanagida, H. Tanaka, T. Kawai, *Bull. Mater. Sc.* **2008**, *31*, 713–717.
- D. Rabelo, E. C. D. Lima, N. Tavares Filho, F. Q. Soares, L. C. Faria, F. Pelegrini, O. Silva, A. C. Oliveira, V. K. Garg, P. C. Morais, *J. Magn. Magn. Mater.* **2004**, *272–276*, E1205–E1206.
- D. Rabelo, F. M. B. Coutinho, *Eur. Polym. J.* **1994**, *30*, 675–682.
- S. B. Oliveira, D. P. Barbosa, A. P. M. Monteiro, D. Rabelo, M. C. Rangel, *Catal. Today* **2008**, *133–135*, 92–98.
- H. Fong, D. H. Reneker, *J. Polym. Sci. B* **1999**, *37*, 3488–3496.
- B. Antic, A. Kremenovic, A. S. Nikolic, M. Stoilkjovic, *J. Phys. Chem. B* **2004**, *108*, 12646–12651.
- A. Kremenovic, B. Antic, V. Spasojevic, M. Vucinic-Vasic, Z. Jaglicic, J. Pirnat, Z. Trontelj, *J. Phys. Condens. Matter* **2005**, *17*, 4285–4299.
- N. Jovic, A. Masadeh, A. Kremenovic, B. Antic, J. Blanus, N. Cvjeticanin, G. Goya, M. Vittori-Antisari, E. Bozin, *J. Phys. Chem. C* **2009**, *113*, 20559–20567.
- M. Vučinić-Vasić, B. Antic, A. Kremenović, A. S. Nikolic, M. Stoilkjovic, N. Bibic, V. Spasojevic, Ph. Colomban, *Nanotechnology* **2006**, *17*, 4877–4884.

46. Z. Cvejc, B. Antic, A. Kremenovic, S. Rakic, G. F. Goya, H. R. Rechenberg, C. Jovalekic, V. Spasojevic, *J. Alloys Compd.* **2009**, 472, 571–575.
47. B. Antic, N. Jovic, M. B. Pavlovic, A. Kremenovic, D. Manojlović, M. Vucinic-Vasic, A. S. Nikolić, *J. Appl. Phys.* **2010**, 107, 043525-1-043525-7.
48. Z. Cvejc, S. Rakic, A. Kremenovic, B. Antic, C. Jovalekic, P. Colombari, *Solid State Sci.* **2006**, 8, 908–915.
49. N. S. Gonçalves, J. A. Carvalho, Z. M. Lima, J. M. Sasaki, *Mater. Lett.* **2012**, 72, 36–38.
50. Z. Zhang, F. Zhou, E. J. Lavernia, *Metall. Mater. Trans. A* **2003**, 34A, 1349–1355.

## Povzetek

Praškovni posnetki 29 vzorcev magnetita, pridobljeni na konvencionalnem difraktometru, so bili uporabljeni za razvoj PLS kalibracijske metode in izbiro spremenljivk za oceno povprečne velikosti kristalitov magnetita direktno iz praškovnih posnetkov. Najboljši IPLS model ustreza Braggovim uklonskim kotom  $35.4^\circ$  ( $h\ k\ l = 3\ 1\ 1$ ),  $43.0^\circ$  ( $h\ k\ l = 4\ 0\ 0$ ),  $53.6^\circ$  ( $h\ k\ l = 4\ 2\ 2$ ) in  $57.0^\circ$  ( $h\ k\ l = 5\ 1\ 1$ ). Najboljši model je GA-PLS, s katerim smo dobili model z RMSEP 0,9 nm in korelacijskim koeficientom 0.9976 med povprečno velikostjo kristalitov izračunano z Williamson-Hallovim pristopom in tisto napovedano z GA-PLS metodo. Dobljeni rezultati kažejo, da lahko napovemo povprečno velikost kristalitov magnetita neposredno iz praškovega posnetka in multivariantne kalibracije z uporabo prostopa PLS izbire spremenljivk.